Nonnegative time–frequency distributions for parametric time–frequency representations using semi-affine transformation group ☆

Hongxing Zou[a,b,c,*], Dianjun Wang[d], Xianda Zhang[a], Yanda Li[a]

[a]*Department of Automation, Tsinghua University, Beijing 100084, China*
[b]*State Key Laboratory of Intelligent Technology and Systems, Tsinghua University, Beijing 100084, China*
[c]*National Laboratory of Pattern Recognition, Institute of Automation, The Chinese Academy of Sciences, Beijing 100080, China*
[d]*Department of Mathematical Sciences, Tsinghua University, Beijing 100084, China*

Abstract

This paper proposes a method for calculating a nonnegative time–frequency distribution (TFD) whose concentration is identical to that of Wigner–Ville distribution (WVD) when instantaneous frequencies (IFs) of the best-matched elementary functions of the signal under analysis are pre-estimated. This method is based on a special class of transformation group, referred to as semi-affine transformation (SAT) group. The essence of this method is to create a joint distribution by translating the values of WVDs of Morlet wavelet to the positions around IFs of the best-matched elementary functions. Theoretical predictions and numerical results indicate that the proposed strategy can result in the most visually appealing TFDs for highly nonstationary signals.
© 2005 Elsevier B.V. All rights reserved.

Keywords: Nonnegative time–frequency distribution; Wigner–Ville distribution; FM[m]let transform; Dopplerlet transform; Semi-affine transformation (SAT) group; Instantaneous frequency; Parametric atomic decomposition; Matching pursuit

*Corresponding author. Department of Automation, Tsinghua University, Beijing 100084, China. Tel.: +8610 62795528; fax: +8610 62786911.

E-mail addresses: hongxing_zou@tsinghua.edu.cn (H. Zou), djwang@tsinghua.edu.cn (D. Wang), zxd-dau@tsinghua.edu.cn (X. Zhang), daulyd@tsinghua.edu.cn (Y. Li).

1. Introduction

Time–frequency representations (TFRs) or time-scale representations (TSRs)[1] was introduced as a tool to characterize the time-varying spectral

---

[1]For convenience, we will forgo the notional distinction between TFR and TSR, treating them as the same. In often a case, the specific name will be clear from context.

contents of nonstationary signals. Despite the substantial achievements of the past 50 years, one of the major issues in the field of TFR has always been which distribution, if any, is the absolute "best" in the sense of cross-term suppression and auto-term concentration. Traditionally, the cross-terms have been mathematically awkward to manipulate. This has made many of the existing TFRs perform inadequately for real applications.

The parametric[2] TFRs seem to be a promising remedy to solve the aforementioned problem. A parametric TFR is the one which decomposes signal over a family of well-localized elementary functions (also known as time–frequency atoms, or *atoms* for short) that are well adapted to the signal's local structures. The polynomial TFRs [4–6], chirplet transform [7–11] and many of its special cases [e.g., the transforms using Gabor elementary functions [12,13], exponential chirplets (hereafter referred to as e-chirplets)[3] [14–18], and Doppler chirplets (d-chirplets) [7,19–22], etc.] are the representatives of the parametric TFRs.

Past theories of parametric TFRs have made great inroads into the problem of cross-term suppression and auto-term concentration mainly by: (1) concentrating on defining various overcomplete sets of model-based elementary functions that exhibit a wide range of time–frequency behaviors, (2) looking for a positive (a misnomer, more strictly, *nonnega-*

tive)[4] and cross-term free time–frequency distribution (TFD) by summing the weighted TFDs [in Cohen's class [26,27], usually the Wigner–Ville distribution (WVD)] of the best-matched elementary functions. But, these endeavors are a complete success only for limited classes of elementary functions—to be more specific, only for the frequency-invariant Gaussian-enveloped elementary functions (e.g., Gabor elementary functions [12,13]), or for the Gaussian-enveloped elementary functions whose frequencies vary linearly with time (e.g., four-parameter Gaussian q-chirplets [10,11]). When the frequencies of the elementary functions vary nonlinearly with time, i.e., the instantaneous frequencies (IFs) of the elementary functions are nonlinear, much of cross-terms will undesirably appear in the final distribution.

In an attempt to alleviate this drawback, we proposed in [14] a "pseudo TFD", obtained by summing the weighted IFs of the best matched Gaussian e-chirplets. Since its marginal in time gives no information of that in frequency and vice versa, this type of representation is by no means a signal's energy distribution. In a parallel development, polynomial TFRs [4–6] give a plausible and interesting result. While meritorious for demonstrating the time-frequency structures of the signal, they are ad hoc, do not completely remove the cross-terms for the most cases, and computing the kernel coefficients is not a trivial task. Hence, more effort needs to be directed in devising a general and tractable formulation of cross-term free TFDs with nonnegativity property. Notice that:

(1) The Gaussian q-chirplet is the only function for which the WVD is nonnegative [28].

(2) Projection of the WVD of a Gaussian q-chirplet onto time–frequency plane is an ellipse.

(3) Projection of the ridge of WVD of a Gaussian q-chirplet onto time–frequency plane is exactly the IF of the Gaussian q-chirplet per se.

(4) The Gaussian q-chirplet is a special case of some other elementary functions, say, a Gaussian e-chirplet. In other words, a Gaussian e-chirplet is

---

[2]In this paper, we use "parametric" TFRs to distinguish those derived from the decompositions using *modeled* elementary functions, where "modeled" means that the elementary function is characterized by several parameters. It is worthwhile noting, however, that the term "parametric" is generally reserved for AR, MA, and ARMA models (see e.g., [1,2] for details). The structured AR model used as a model-based time–frequency distribution (TFD) can be found in [3].

[3]The "chirplet" is a noun of multitude. The commonly used chirplets include [7]: w-chirplet (warbling chirplet), p-chirplet (projective chirplet used in image processing), q-chirplet (quadratic chirplet, i.e., quadratic phase), and d-chirplet (Doppler chirplet). In [14–18], we refer to the *dilated and translated windowed exponential frequency-modulated elementary function* as "FM^m let". In this paper, we prefer this terminology to "exponential chirplet (e-chirplet)" since, in principle, the FM^m let can be fitted in the framework of chirplet. Likewise, the "Dopplerlet" in [19–22] can be referred to as "d-chirplet".

[4]There has been a great surge of activities in the past 20 years or so on the distribution functions which are everywhere nonnegative on the premise that such functions are more closely parallel to their classical counterparts. The initial impetus came from the original work by Cohen and Posch [23], and later work by Loughlin et al. [24], Sang et al. [25], and others.

a frequency-modulated version of a Gaussian q-chirplet [17]. Moreover, a Morlet wavelet is also a special case of Gaussian q-chirplet, therefore a Gaussian e-chirplet is also a frequency-modulated version of a Morlet wavelet [17].

(5) Frequency modulation $s(t)e^{j\phi(t)}$ of signal $s(t)$ in the time domain gives rise to a shearing or warping in the time–frequency plane, but does not alter the signal's instantaneous power [because $|s(t)e^{j\phi(t)}|^2 = |s(t)|^2|e^{j\phi(t)}|^2 = |s(t)|^2$] and, accordingly, does not affect the time marginal property and the total energy.

Then, intuitively, if we can devise a surrogate TFD by moving the values of WVDs of Morlet wavelets to the positions of IFs of the best-matched Gaussian e-chirplets, we can readily obtain a nonnegative and cross-term free TFD (NN-TFD). Fig. 1 is a somewhat typical illustration to this idea, showing how the WVD (constrained in a dashed parallelogram) of a Morlet wavelet migrates parallel along the frequency axis only. Geometrically, this migration, which we call the *semi-affine transformation* (*SAT*) *of time–frequency plane*, adapts the new TFD (namely,

Fig. 1. SAT of time–frequency plane. The ellipse (shape of WVD of Morlet wavelet in time–frequency plane) adaptively "warps" in accordance with the difference of IF laws between a Gaussian e-chirplet and a Morlet wavelet. In the usual context, the abscissa and ordinate (not displayed) of this plot correspond to time and frequency, respectively. We have deliberately eliminated the coordinates, recognizing that, for any operation in the time domain, there is an equivalent operation in the frequency domain, or in the scale domain, or in whatever other reasonable coordinate space in which one might wish to work.

NN-WVD) in time–frequency plane in such a way as to fit the IF of the best-matched e-chirplet. We note that similar ideas of migration can also be found in the *reassignment* method [29–31], which improves the "readability" of a TFD by creating a modified version of the TFD based on the trick of movement of its values away from where they are computed. Also note that for signals that are both frequency and amplitude modulated, a class of distributions which are explicit functionals of the IF can be found in [32].

This paper is a sequel to [33] and presents novel results on NN-WVD within the framework of SAT. The remainder of this paper is organized as follows. In Section 2 we introduce the SAT which underlies our subject. As an illustration of how to devise an NN-WVD for a specific parametric TFR, a synopsis of the e-chirplet transform is presented in Section 3 and the details for devising the NN-WVD for the e-chirplet transform is described in Section 4. Three examples for which the NN-WVD is evidently appealing are given in Section 5 and our conclusions are drawn in Section 6. Throughout the paper, we assume that any real-valued signal under analysis can be converted to a complex signal via the Hilbert transform or other filtering techniques.
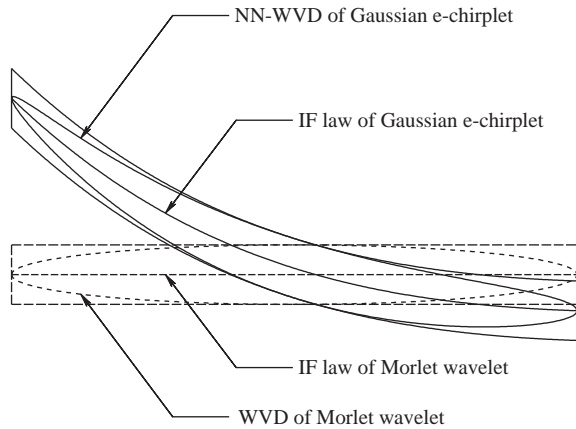
2. Semi-affine transformation of time–frequency plane

In Section 4, we need to find an explicit expression of NN-WVD. Toward this end, we introduce a kind of transformation of time–frequency plane. Such a transformation (refer to Fig. 1) can be rigorously defined as follows:

Definition 1. Let $a \in \mathbb{R}$, where $\mathbb{R}$ denotes the set of real numbers. Let $\zeta(t)$ be a continuous function over $\mathbb{R}$. Define a semi-affine transformation (SAT) $\Xi_{a,\zeta}$ in the time–frequency plane $(t,f) \in \mathbb{R}^2$ such that

$$\Xi_{a,\zeta}(t,f) = (t, f + \zeta(t) - a), \quad (t,f) \in \mathbb{R}^2 \quad (1)$$

which portrays the action of $\Xi_{a,\zeta}$ as a nonlinear transformation mapping $\mathbb{R}^2$ into $\mathbb{R}^2$. As can be seen from (1), under the SAT $\Xi_{a,\zeta}$, a given point

(t, f) on the time–frequency plane is migrated to a new point $(t, f + \zeta(t) - a)$. Note that this migration is parallel to the frequency axis only, hence the name *semi-affine transformation* because of its departure from the stringent "parallelity" of two lines in affine transformation.

Remarks. (1) If $\Xi_{a,\zeta}(t_1, f_1) = \Xi_{a,\zeta}(t_2, f_2)$, then it follows from (1) that $t_1 = t_2$, $f_1 + \zeta(t_1) - a = f_2 + \zeta(t_2) - t_2 = f_2 + \zeta(t_1) - a$, and $f_1 = f_2$. This implies that $\Xi_{a,\zeta}$ is injective, i.e., if $(t_1, f_1) \neq (t_2, f_2)$, then, $\Xi_{a,\zeta}(t_1, f_1) \neq \Xi_{a,\zeta}(t_2, f_2)$. For all $(t, f) \in \mathbb{R}^2$, it is easily found that $\Xi_{a,\zeta}(t, f - \zeta(t) + a) = (t, f)$, therefore, the SAT $\Xi_{a,\zeta}$ given by Definition 1 is surjective. Thus, $\Xi_{a,\zeta}$ is a one-to-one transformation in the time–frequency plane.

(2) If $\xi(t) = \zeta(t) + b$, one observes that

$$\Xi_{a,\xi}(t, f) = (t, f + \xi(t) - a)$$
$$= (t, f + \zeta(t) - (a - b)) = \Xi_{a-b,\zeta}(t, f).$$

This means that $\Xi_{a,\zeta}$ is not uniquely determined by $\zeta(t)$. In general, $\Xi_{a,\zeta} = \Xi_{b,\xi}$, if and only if $\zeta(t) - \xi(t) = a - b$, $t \in \mathbb{R}$.

(3) Geometrically, the SAT $\Xi_{a,\zeta}$ is to topologically transform a 2-D phase plane $\Phi(t, f)$ to another phase plane $\Phi'(t, f')$, where $f' = f + \zeta(t) - a$. (Refer to Fig. 1.)

In order for one to understand the SAT $\Xi_{a,\zeta}$ in a meaningful sense, let us see a simple example. Referring to Fig. 1, suppose that $\zeta(t) = t^2 + 2t$, $a = 0$, and an ellipse is given by

$$\left(\frac{f}{b_1}\right)^2 + \left(\frac{t}{b_2}\right)^2 = 1.$$

Under the SAT $\Xi_{a,\zeta}$, this ellipse is mapped to the following new function

$$\left[\frac{f + (t^2 + 2t)}{b_1}\right]^2 + \left(\frac{t}{b_2}\right)^2 = 1,$$

which, as we can see, is not an ellipse any more.

The following are some superficial but fundamental properties[5] of $\Xi_{a,\zeta}$.

---

[5]We will not discuss the plethora of algebraic properties nor the fascinating topological properties of SAT and its corresponding group, which—among other things—will be discussed at length in our forthcoming paper.

Property 1.. If curve $f = \zeta(t)$ intersects $f = \xi(t)$, then $\Xi_{a,\zeta} = \Xi_{b,\xi}$ if and only if $a = b$ and $\zeta(t) = \xi(t)$, $t \in \mathbb{R}$.

Property 2.. If $a \in \mathbb{R}$, $b \in \mathbb{R}$, $\zeta(t)$ and $\xi(t)$ are continuous functions over $\mathbb{R}$; then, $\Xi_{a,\zeta} \cdot \Xi_{b,\xi} = \Xi_{a+b,\zeta+\xi}$.

Proof of Property 2.

$$\Xi_{a,\zeta} \cdot \Xi_{b,\xi}(t, f) = \Xi_{a,\zeta}(t, f + \xi(t) - b)$$
$$= (t, f + \zeta(t) + \xi(t) - (a + b))$$
$$= \Xi_{a+b,\zeta+\xi}(t, f), \quad (t, f) \in \mathbb{R}^2.$$

This completes the proof of Property 2. $\square$

Property 3.. $\Xi_{a,\zeta} \cdot \Xi_{b,\xi} = \Xi_{b,\xi} \cdot \Xi_{a,\zeta}$, i.e., the multiplication satisfies the commutative law.

Denote all the SATs $\{\Xi_{a,\zeta}\}$ by G, that is,

$$G = \{\Xi_{a,\zeta} \mid a \in \mathbb{R}, \ \zeta(t) \text{ is continuous over } \mathbb{R}\}. \quad (2)$$

Theorem 1. *The set G forms a commutative group with the multiplication of transformations.*

Proof of Theorem 1. We need only prove the existence of an identity element and an inverse element. Since $\Xi_{0,0}\Xi_{a,\zeta} = \Xi_{a,\zeta}$, G has identity elements. Furthermore, $\Xi_{a,\zeta}^{-1} = \Xi_{-a,-\zeta} \in G$, therefore every element of G has an inverse. It follows from Property 3 and the associative law of multiplication that G forms a commutative group with the multiplication of transformations. $\square$

The set G defined in (2) is now called *SAT group*.

Theorem 2. *Let*

$$H = \{\Xi_{a,\zeta} \mid a \in \mathbb{R}, \ \zeta(t) \text{ is differentiable over } \mathbb{R}\}.$$

Then, (a) *H is a subset of G, and* (b) *H is an area-preserved transformation group.*

Proof of Theorem 2. It is easy to see that H is a subgroup of G. To show (b), let $\Xi_{a,\zeta} \in H$, $\Xi_{a,\zeta} : t \mapsto u(t, f) = t, f \mapsto v(t, f) = f + \zeta(t) - a$. Since

the transformation Jacobian

$$J = \frac{\partial(u,v)}{\partial(t,f)} = \begin{vmatrix} \dfrac{\partial u}{\partial t} & \dfrac{\partial u}{\partial f} \\[2mm] \dfrac{\partial v}{\partial t} & \dfrac{\partial v}{\partial f} \end{vmatrix} = \begin{vmatrix} 1 & 0 \\ \zeta'(t) & 1 \end{vmatrix} \equiv 1,$$

consequently, each transformation in subgroup H preserves the area. $\square$

Theorem 2 has a rather useful practical consequence. From this theorem it follows that (1) the time–frequency concentration is not affected under the SAT (taking advantage of the fact that the SAT is area preserving), (2) the energy conservation property is reserved under the SAT (taking advantage of another fact that the SAT does not alter the magnitude of the original time–frequency plane).

3. Outline of e-chirplet transform

The e-chirplet [14] is defined by

$$q_{t_c,f_c,\log\sigma,r,m}(t)$$
$$= \frac{1}{\sqrt{\sigma}} g\left(\frac{t - t_c}{\sigma}\right)$$
$$\times \exp\left\{ j2\pi \left[1 + r\left(\frac{t - t_c}{\sigma}\right)\right]^m f_c\left(\frac{t - t_c}{\sigma}\right) \right\}, \quad (3)$$

where $j = \sqrt{-1}$, $(t_c, f_c, \log\sigma, r, m)$ represent the parameters, $\sigma \in \mathbb{R}^+$, $(t_c, f_c, r, m) \in \mathbb{R}^4$; $g(t)$ is the window function (also known as "mother e-chirplet"), t_c the time-center, f_c the frequency-center, $\log\sigma$ the log-duration, r the chirprate, and m the FM exponent. The IF of (3) is given by

$$\text{IF}_q(t) = \frac{1}{2\pi} \frac{d[\arg\{q_{t_c,f_c,\log\sigma,r,m}(t)\}]}{dt}$$
$$= \frac{1}{\sigma} \left[1 + (1 + m)r\left(\frac{t - t_c}{\sigma}\right)\right]$$
$$\times \left[1 + r\left(\frac{t - t_c}{\sigma}\right)\right]^{m-1} f_c. \quad (4)$$

As remarked in [14], Eq. (3) is the prototype of the elementary functions of many other transforms. For example, the wavelet is a special case of an e-chirplet where $m = 0$; the q-chirplet is a peculiar circumstance of an e-chirplet granted that $m = 1$.

Once the e-chirplets are used as elementary functions, the e-chirplet transform of any measurable and square-integrable signal $s(t) \in L^2(\mathbb{R})$ may be readily defined as

$$\text{ECT}_s(\gamma) = \langle s, \ q_\gamma \rangle, \quad (5)$$

where $\gamma = (t_c, f_c, \log\sigma, r, m)$ represents the parameter list and "$\langle, \rangle$" denotes the Dirac inner product.

The implementation of e-chirplet transform is based on the *matching pursuit* due to Mallat [13], and we devote a few lines to evoke the procedure for later use. Similar procedures can also be found in [10–12,34]. A matching pursuit algorithm is the one that *adaptively* decomposes any signal under analysis into a linear combination of a set of elementary functions that are selected from a large redundant (overcomplete) dictionary of elementary functions in accordance with the criterion of maximum projection energy. These elementary functions are chosen in order to best match the signal's local structures. Note that representing a signal using an overcomplete dictionary of elementary functions is an inspiring challenge. Besides the matching pursuit, several other algorithms have also been proposed to attack this representation and to measure its optimality, see e.g., Daubechies' *method of frames* [35], Coifman's *best basis* [36], and Chen and Donoho's *basis pursuit* [37].

Let $\mathbf{H}$ denote a Hilbert space, $\mathscr{D} = \{q_\gamma\}_{\gamma\in\Gamma}$ be a dictionary of vectors in $\mathbf{H}$ with $\|q_\gamma\| = 1$ (where the index γ stands for the parameter list and Γ for the parameter space). Let $s \in L^2(\mathbb{R})$, $q_{\gamma_0} \in \mathscr{D}$; then, the signal s can be decomposed into

$$s = \langle s, \ q_{\gamma_0} \rangle q_{\gamma_0} + R_s, \quad (6)$$

where $\langle s, \ q_{\gamma_0} \rangle q_{\gamma_0}$ is the projection of s in the direction of q_{γ_0}, R_s is its corresponding residual signal. The matching-pursuit-based e-chirplet transform is an *iterative* projection algorithm that subdecomposes the residual signal R_s by projecting it on a vector of $\mathscr{D}$ that matches R_s almost at best, as was done for s in (6). After each iteration, an e-chirplet that best matched the dominating component of residual signal is selected. The decomposition process is iterated until the residual energy is below some threshold or until some other

halting criterion is met. Let $R_s^{(0)} = s$. Suppose that we have finished k iterations; then, at the end of $(k+1)$th iteration we obtain[6]

$$
\begin{aligned}
R_s^{(0)} &= \sum_{i=0}^{k} \langle R_s^{(i)},\ q_{\gamma_i} \rangle q_{\gamma_i} + R_s^{(k+1)} \\
&= \sum_{i=0}^{k} A_i q_{\gamma_i} + R_s^{(k+1)},
\end{aligned}
\tag{7}
$$

where $A_i = \langle R_s^{(i)},\ q_{\gamma_i} \rangle$, $\gamma_i = (t_c^{(i)}, f_c^{(i)}, \sigma^{(i)}, r^{(i)}, m^{(i)})$ represents the parameter list of the ith e-chirplet. Since the energy of residual signal $\|R_s^{(k+1)}\|^2$ monotonically decreases as k increases [13], i.e., $\lim_{k \to +\infty} \|R_s^{(k+1)}\|^2 = 0$ (provided that the number of samples is finite), it follows that

$$
s = \sum_{i=0}^{+\infty} A_i q_{\gamma_i},
\tag{8}
$$

which is the formulation of the *inverse* e-chirplet transform.

4. Devising NN-WVD for e-chirplet transform

4.1. Theoretical derivation

The WVD of signal $s(t) \in L^2(\mathbb{R})$ is defined by

$$
W_s(t,f) = \int_{-\infty}^{\infty} s\left(t + \frac{\tau}{2}\right) s^*\left(t - \frac{\tau}{2}\right) e^{-j2\pi f \tau} \, d\tau.
\tag{9}
$$

It is now clear that the WVD is the standard framework around which numerous TFDs are fashioned. The WVD has many desirable properties and the ability to provide remarkable concentration in time and frequency, which distinguishes the WVD from its counterparts.

Since the WVD of e-chirplet $q_\gamma(t)$ does not have a simple, closed-form expression, we consider

hereafter the special case $w(t)$, where $w(t) = q_\gamma(t)|_{m=0}$ (i.e., the wavelet case). If $m = 0$ and the window function $g(t)$ is a normalized Gaussian function

$$
g_{t_c, \sigma}(t) = (\pi \sigma^2)^{-1/4} \exp\left\{ -\frac{1}{2}\left(\frac{t - t_c}{\sigma}\right)^2 \right\},
$$

then (3) will reduce to a Morlet wavelet[7]

$$
\begin{aligned}
w_{t_c, f_c, \log \sigma}(t) = {} & (\pi \sigma^2)^{-1/4} \exp\left\{ -\frac{1}{2}\left(\frac{t - t_c}{\sigma}\right)^2 \right\} \\
& \times \exp\left\{ j2\pi f_c\left(\frac{t - t_c}{\sigma}\right) \right\},
\end{aligned}
\tag{10}
$$

and (4) to a horizontal straight line

$$
\mathrm{IF}_w(t) = \frac{f_c}{\sigma}.
\tag{11}
$$

The WVD of (10) is given by

$$
W_w(t,f) = 2 \exp\left\{ -(\sigma f - 2\pi f_c)^2 - \left(\frac{t - t_c}{\sigma}\right)^2 \right\},
\tag{12}
$$

which has elliptically shaped equiprobability contours in the time–frequency plane. The contour for the case where the levels are down to $1/C$ (where C is a constant, $C > 1$) of their peak value A [$A = 2$ as per (12)], is an ellipse, which is given by

$$
\left(\frac{f - 2\pi f_c/\sigma}{\sqrt{\log C}/\sigma}\right)^2 + \left(\frac{t - t_c}{\sqrt{\log C}\,\sigma}\right)^2 = 1,
\tag{13}
$$

---

[6]If there appears to be any chance of confusion with the power of a quantity, we will enclose the superscript in parentheses to secure on a sound mathematical footing. Thus, in what follows, $R_s^{(i)}$ designates the ith residual signal, whereas α^i designates α to the power i. Moreover, we also use a subscript to denote a quantity with a specific nature (e.g., t_c, where the subscript c refers to center). This unfortunate notation may create confusion with, say, γ_i but, fortunately, the subscript i is traditionally reserved for the ith quantity; hence, γ_i refers to the ith parameter set.

[7]The *Morlet* mother wavelet is rigorously defined as

$$
\pi^{-1/4} \exp\{-t^2/2\}[\exp\{j2\pi f_c t\} - \exp\{-(2\pi f_c)^2/2\}],
$$

where f_c is the center-frequency of the mother wavelet. The second term in brackets is known as the correction term, as it corrects for the nonzero mean of the complex sinusoid of the first term. In practice, it becomes negligible for values of $f_c \gg 0$ and can be ignored, in which case, the Morlet mother wavelet can be written in a simple form as

$$
\pi^{-1/4} \exp\{-t^2/2\} \exp\{j2\pi f_c t\}.
$$

This wavelet is simply a complex sinusoid within a Gaussian envelope. Note that the simple Morlet mother wavelet is not strictly a wavelet as it has nonzero mean, i.e., the zero frequency term of its corresponding energy spectrum is nonzero and hence it is inadmissible. However, it can be used in practice with $f_c \gg 0$ with minimal error. A more detailed overview of the definitions of wavelet functions can be found in [38].

with its radii of major axes given by

$$l_T = \sqrt{\log C}\, \sigma, \quad l_F = \sqrt{\log C}/\sigma. \tag{14}$$

To find the explicit expression of NN-WVD for the ith e-chirplet, we simply perform the SAT $\Xi_{a,\zeta}$ on the WVD (12) of the ith Morlet wavelet, yielding

$$\begin{aligned}
\varpi_{q_{\gamma_i}}(t,f) &= W_{w_i}(\Xi_{a^{(i)},\zeta^{(i)}(t)}(t,f)) \\
&= W_{w_i}(t, f + \zeta^{(i)}(t) - a^{(i)}) \\
&= 2\exp\Big\{ -[\sigma^{(i)}(f + \zeta^{(i)}(t) - a^{(i)}) \\
&\quad -2\pi f_c^{(i)}]^2 - \left(\frac{t - t_c^{(i)}}{\sigma^{(i)}}\right)^2 \Big\},
\end{aligned} \tag{15}$$

where $\zeta^{(i)}(t) = \mathrm{IF}_{q_{\gamma_i}}$ [refer to (4)] and $a^{(i)} = \mathrm{IF}_{w_i}(t) = f_c^{(i)}/\sigma^{(i)}$ [refer to (11)].

If a signal $s(t)$ has P the best-matched elementary functions (provided that we have performed P iterations of decomposition), then we immediately have

$$\varpi_s(t,f) = \sum_{i=0}^{P-1} |A_i|^2 \cdot \varpi_{q_{\gamma_i}}(t,f), \tag{16}$$

which can be paraphrased as follows: For each iteration, we get a different best-matched e-chirplet and a corresponding NN-WVD, the totality of these NN-WVDs gives us a TFD for the signal under analysis.

4.2. Implementation

We have implemented a straightforward algorithmic procedure in MATLAB$^{®}$ that allows to calculate the NN-WVD of any Gaussian windowed parametric elementary function. The tractable algorithm proceeds as follows:

NN-WVD Algorithm
1. **Initialization**: Generate an L-by-L matrix of zeros $\varpi_s(t,f)$, where L is the length of the signal $s(t)$.
2. **E-Chirplet transform**: Calculate the e-chirplet transform based on matching pursuit, save the resulting parameters for P matched e-chirplet: A_i, $\gamma_i = (t_c^{(i)}, f_c^{(i)}, \sigma^{(i)}, r^{(i)}, m^{(i)})$, $i = 0, 1, 2, \ldots, P - 1$.

3. **Calculate NN-WVD**: For iterations $i = 0, 1, 2, \ldots, P - 1$
   (1) Generate an L-by-L matrix of zeros $\varpi_{q_{\gamma_i}}(t,f)$;
   (2) Calculate the $\zeta^{(i)}(t) = \mathrm{IF}_{q_{\gamma_i}}(t)$ for ith e-chirplet using (4);
   (3) Calculate $a^{(i)} = \mathrm{IF}_{w_i}(t)$ for ith Morlet wavelet using (11);
   (4) Calculate the $W_{w_i}(t,f)$ for ith Morlet wavelet $w_i(t)$ using (12);
   (5) Determine the lengths of two neighboring sides of the parallelogram surrounding $W_{w_i}(t,f)$ according to (14) as $2l_T^{(i)}$ and $2l_F^{(i)}$, respectively;
   (6) Calculate the $\varpi_{q_{\gamma_i}}(t,f)$ for ith e-chirplet $q_{\gamma_i}(t)$ using (15). This step can be done simply as follows [other than directly manipulating (15)]. At each time instant t, $t \in [t_c^{(i)} - l_T^{(i)}, t_c^{(i)} + l_T^{(i)}]$, let $\varpi_{q_{\gamma_i}}(t,f) = W_{w_i}(t,f')$, where
   $f \in [\mathrm{IF}_{q_{\gamma_i}}(t) - l_F^{(i)},\ \mathrm{IF}_{q_{\gamma_i}}(t) + l_F^{(i)}]$,
   $f' \in [\mathrm{IF}_{w_i}(t) - l_F^{(i)},\ \mathrm{IF}_{w_i}(t) + l_F^{(i)}]$;
   (7) $\varpi_s(t,f) = \varpi_s(t,f) + |A_i|^2 \cdot \varpi_{q_{\gamma_i}}(t,f)$.

5. Examples

This section presents three application results using two kinds of highly nonstationary signals in support of the methodology advocated. The first example performs a qualitative comparison between the e-chirplet-based NN-WVD, the STFT-based spectrogram, the WVD, and the q-chirplet-based WVD using a bat sonar signal. The next two examples compare the analysis results of WVD with that of NN-WVD using a computer-generated Doppler signal and a recorded real-world Doppler signal, respectively.

Example 1. It is difficult to compare different methods for computing TFDs since there is no clear measure of the "goodness" of a TFD, we will present pictures of the TFDs obtained by using different methods and provide a qualitative comparison of their abilities to characterize the signal's time-varying structures. In order to achieve as fair a comparison as possible, the dynamic ranges of the images are the same within each TFD. Now that the 2.5 ms echolation pulse

emitted by the large brown bat *Eptesicus fusus* is becoming the de facto standard signal for evaluating the merit of a proposed TFD in the realm of time–frequency analysis (the signal is highly nonstationary). Just like the "Lena" image for benchmarking different approaches to image processing, we will test different TFDs with this bat sonar signal. Fig. 2(a) depicts the waveform of the bat sonar signal (with a normalized time–bandwidth product $T \times B = 226.7643 \gg 1$). Fig. 2(b) is the STFT-based spectrogram (squared magnitude of STFT) with a Hamming window of length 101 points. A common shortcoming with spectrograms is however their poor time–frequency concentration. Fig. 2(c) illustrates the WVD. The time–frequency concentration of WVD is considered to be optimal, but its inherent cross-term interference can adversely affect its performance and may potentially lead to confusion and misinterpretation. Note that both the spectrogram and the WVD show how the frequency components of the signal change over time, but both of them produce some seemingly bizarre results, which are nonetheless true because of their inherent cross-terms. Fig. 2(d) plots a decomposition result of the four parameter q-chirplet transform [10,11]. Although this sort of TFD (obtained by summing the WVDs of the first five weighted matched Gaussian q-chirplets) is nonnegative and has optimal time–frequency concentration, the distortion in characterizing the time-varying structures is also salient, since, as can be seen from Figs. 2(b) and (c), two components of the bat sonar signal are inherently not the q-chirplets, they are more like the *whistlers* or *gliding tones*. Circumventing this drawback was a major motivation for our proposing the e-chirplet transform. The energy of the corresponding residual signal is 8.75% better than that reported in [10] (where the value is 10% and ten Gaussian q-chirplets are needed). Fig. 2(e) is the decomposition results based on the Gaussian e-chirplet transform, that is obtained by directly summing the NN-WVDs of the first five matched Gaussian e-chirplets. As can be seen in this example, the resulting distribution outperforms the spectrogram, WVD, and q-chirplet transform and, therefore, offers a better understanding of the nature of

the bat sonar signal. Fig. 2(f) plots the residual signal (obtained by subtracting the first five weighted matched Gaussian e-chirplets from the original signal), where the ratio between the energy of the remainder and that of the original signal is 7.06%.

Example 2. The d-chirplet (for the subsonic case) [19–22] is a windowed, translated, and dilated Doppler signal defined by[8]

$$
\begin{aligned}
d_\gamma(t) &= d_{t_c, f_c, \log \sigma, l, v, u}(t) \\
&= \frac{1}{\sqrt{\sigma}} g\left(\frac{t - t_c}{\sigma}\right) \\
&\quad \times \exp\left\{ j 2\pi u \left[u + \frac{v^2(t - t_c/\sigma)}{\sqrt{l^2 + v^2(t - t_c/\sigma)^2}} \right]^{-1} \right. \\
&\quad \left. \times f_c\left(\frac{t - t_c}{\sigma}\right) \right\}.
\end{aligned}
\tag{17}
$$

Clearly, such an elementary function is dictated by, besides the shape of window function $g(t)$ (also known as "mother d-chirplet"), the following six free parameters each of which has an intuitively satisfying physical significance: time-center t_c, frequency-center f_c, log-duration $\log \sigma$, distance l between the observer and the line that the source moves along, source speed v, and wave propagation speed u.

A joint time–frequency analysis of such an elementary function when $g(t)$ is Gaussian, is plotted in Fig. 3, where the TFD is WVD. As can be seen from this figure, although the signal component is well concentrated in the time-frequency plane, numerous cross-terms appear at positions in time and frequency, where the energy is expected to be null.

To devise an NN-WVD for the d-chirplet signal, we use the same procedure as narrated in Section 4. The main differences between an

---

[8]In [7], Mann describes another three-parameter d-chirplet representation that models a source producing a sinusoidal wave while moving along a straight line. The three parameters are center frequency, maximum rate of change of frequency, and frequency swing.
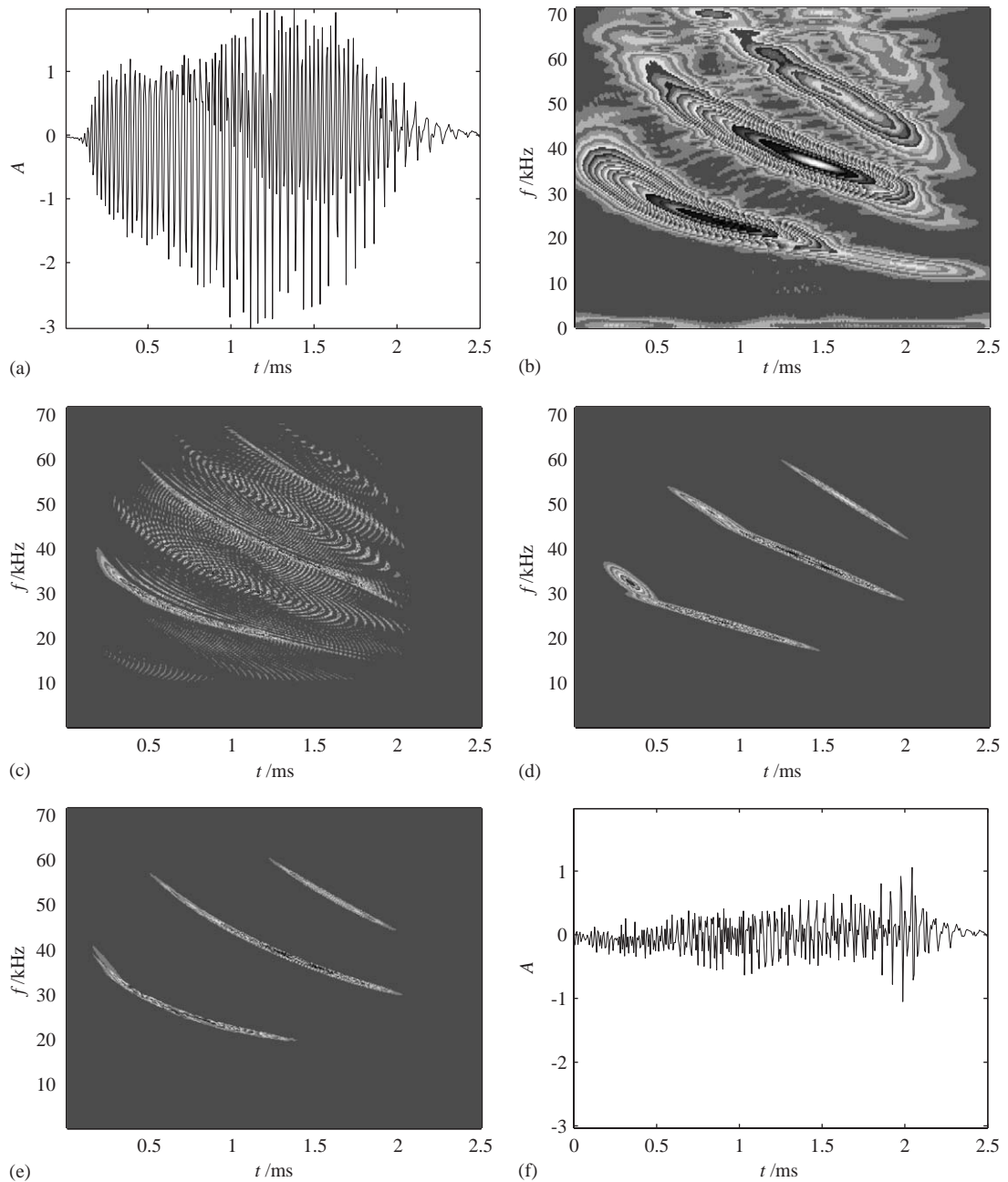
Fig. 2. Bat sonar signal and its TFDs: (a) waveform; (b) STFT-based spectrogram; (c) WVD; (d) q-chirplet-transform-based WVD; (e) e-chirplet-transform-based NN-WVD; (f) residual signal (Data courtesy of http://www-dsp.rice.edu/software/tfa.shtml).

e-chirplet and a d-chirplet are the number of parameters and the frequency behavior of their IFs. By referring to (17) we see that, if the source

speed $v = 0$, then the Gaussian d-chirplet will reduce to Morlet wavelet. As explained in Section 1, the instantaneous powers of a wavelet
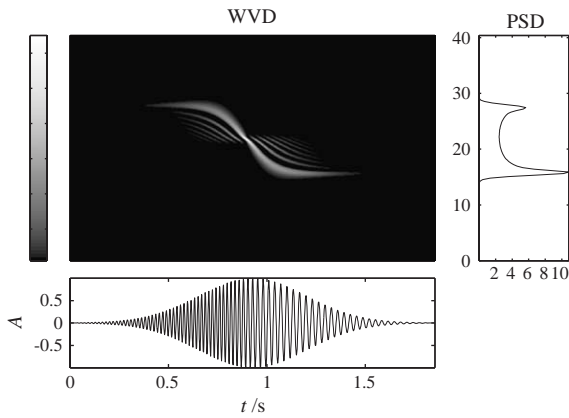
Fig. 3. Joint time–frequency analysis, showing the traditional power spectral density [(PSD), obtained using Welch's averaged periodogram method] to the right of and time waveform below the WVD of a Gaussian d-chirplet. The cross-terms of the WVD are troublesome both in analysis and synthesis.
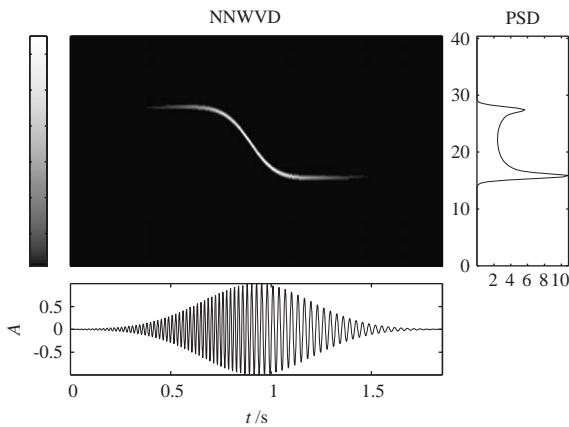

Fig. 4. Joint time–frequency analysis, showing the PSD to the right of and time waveform below the NN-WVD of the same Gaussian d-chirplet used in Fig. 3. The cross-terms now disappear while simultaneously the auto-term is optimally reserved.

and a d-chirplet are identical if their window functions are the same. Fig. 4 displays the NN-WVD of the same Gaussian d-chirplet signal, that yields a nonnegative and cross-term free TFD with its concentration identical to that of WVD. Note that the same issue is discussed in [6], where the sixth- and eighth-order polynomial WVDs, respectively, are used for a Doppler signal, but, unfortunately, the cross-terms are still present and noticeable.
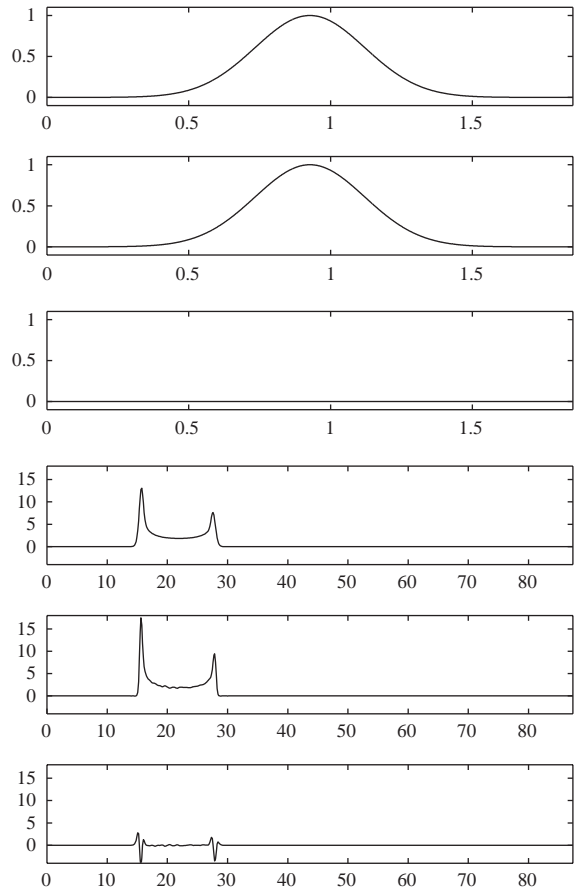

Fig. 5. From top to bottom: time marginal of WVD, time marginal of NN-WVD, difference between the two time marginals (which is zero everywhere), frequency marginal of WVD, frequency marginal of NN-WVD, and the difference between the two frequency marginals of the signal shown in both Figs. 3 and 4. For the first three subfigures, the horizontal axis corresponds to time (in s) and the vertical axis to magnitude. For the last three subfigures, the horizontal axis corresponds to frequency (in Hertz) and the vertical axis to energy spectral magnitude. As can be seen from this figure, after semi-affine transforming the time–frequency plane, only the time marginal is exactly preserved; the frequency marginal is only approximately retained.

Fig. 5 shows (from top to bottom), respectively, the time marginal of WVD [defined by $\int_{-\infty}^{\infty} W_s(t,f)\,df$], time marginal of NN-WVD [defined by $\int_{-\infty}^{\infty} \varpi_s(t,f)\,df$], difference between the two time marginals, frequency marginal of WVD [defined by $\int_{-\infty}^{\infty} W_s(t,f)\,dt$], frequency

marginal of NN-WVD [defined by $\int_{-\infty}^{\infty} \varpi_s(t,f)\,dt$], and the difference between the two frequency marginals of the signal $s(t)$ shown in both Figs. 3 and 4. As can be seen from this figure, the time marginal of NN-WVD is identical to that of WVD (this is a direct consequence of Theorem 2) and both of them are identical to the instantaneous power (as stated in Section 1); the frequency marginal of NN-WVD slightly differs from that of WVD. The energy of WVD [defined by $\int_{-\infty}^{\infty}\int_{-\infty}^{\infty} W_s(t,f)\,dt\,df$] is 340.0334 and the energy of NN-WVD [defined by $\int_{-\infty}^{\infty}\int_{-\infty}^{\infty} \varpi_s(t,f)\,dt\,df$] is 340.0332; hence, a preservation of energy conservation property under the SAT (as anticipated by Theorem 2).

Example 3. In this example, we consider a more realistic application of NN-WVD for measuring the Doppler-shifted frequencies.

To help illustrate the experiment system, a schematic diagram is shown in Fig. 6. We carried out the experiment in a day May, 1–5 h after a thunder storm. The car moved along a straight line at a constant speed 19.5 m/s (which was obtained from averaging the GPS speed data) and a loudspeaker (mounted on a car) emitted a 3003-Hz pure tone. During the time of recording, the temperature was 18.5 °C, barometric pressure was 99 414 Pa, and the relative humidity was 67.5%, therefore, the theoretical sound speed for the given atmospheric data was 343.3 m/s. (For an easy reference of how to calculate the sound speed, see Appendix C.A of [22].)

Fig. 7 displays the WVD of the recorded sound signal. As can be seen in this figure, the signal of interest is embedded in a strong background noise so that it is very difficult for WVD to resolve it. Since the sound sources (including the loudspeaker, rotating and vibrating machinery parts of the moving car, and the friction between the car and air, etc.) generate the same frequency warping laws (note that these frequency warping laws differ only by their center-frequencies and center-times), in our case of estimation of range and speed using the d-chirplet transform, only one dominating signal component is sufficient for estimating the range and speed of the sound source. This means that we need only perform the iteration once. The dominating signal component is automatically searched because of the intrinsic
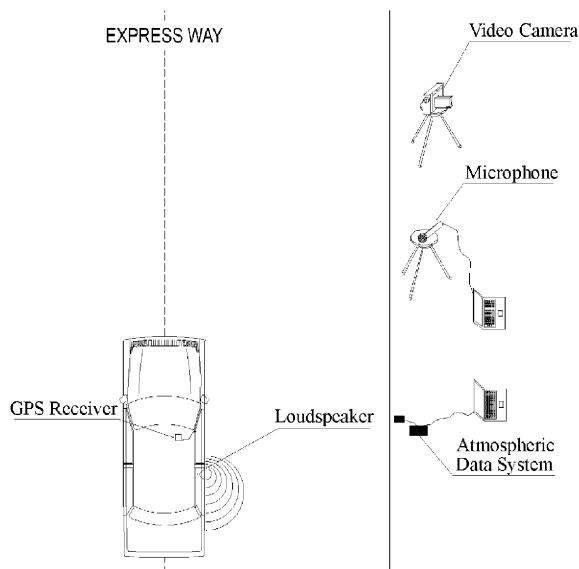

Fig. 6. Arrangement for measuring the motion parameters of a car moving in a straight path.
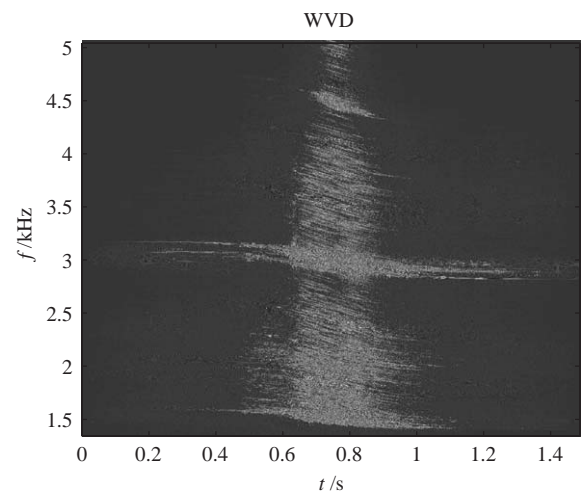

Fig. 7. WVD of an airborne acoustic signal. The WVD is a smudged blur and an incomprehensible mess due to the notorious cross-terms and background noise (mechanical rotation and vibration of the moving car, friction between car and air, traffic noise, and the rustle of leaves, etc.). It is very hard to estimate the Doppler-shifted frequencies from this figure, or to see what really happened in the vicinity of time-center and frequency-center.

selection mechanism of maximum projection energy of the matching pursuit algorithm.

Fig. 8 graphs the NN-WVD of the matched dominating signal component. Comparing Fig. 8 with Fig. 7 we see that the WVD in Fig. 7 is incomprehensible due to cross-terms and background noise, whereas the NN-WVD shown in Fig. 8 is everywhere nonnegative and clearly depicts the time-varying nature of the signal. The Doppler-shifted frequencies can be read directly from the NN-WVD using the cross-cursor as 3181 and 2847 Hz, respectively, on account of the clear visual appearance and high time–frequency concentration of the NN-WVD. From the sound speed $u = 343.3$ m/s and the Doppler-shifted frequencies

$$\frac{f_c}{1 - v/u} = 3181\,\text{Hz}, \quad \frac{f_c}{1 + v/u} = 2847\,\text{Hz},$$

we immediately know that the car moved at a constant speed of 19.0 m/s and the loudspeaker emitted a wave of frequency 3004 Hz, all of which agreed very closely with the accurately monitored real data.
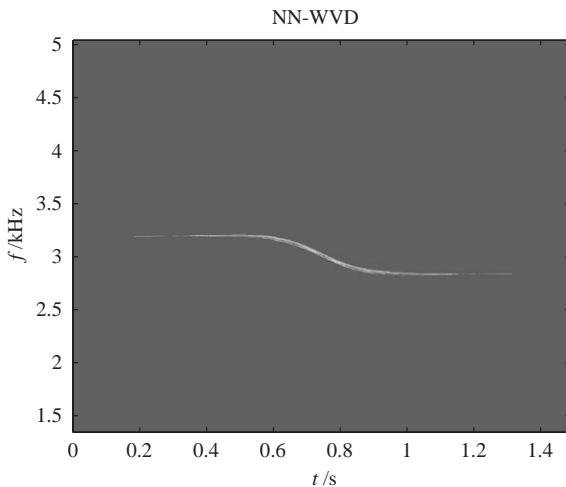

Fig. 8. NN-WVD of the matched dominating signal component of the airborne acoustic signal shown in Fig. 7. The NN-WVD is nonnegative everywhere and clearly depicts how the frequency contents of the interested signal vary with time. The Doppler-shifted frequencies can be read directly from the NN-WVD as 3181 and 2847 Hz.

6. Concluding remarks

In this paper, we proposed a new group called "semi-affine transformation (SAT) group" and devised a new TFD called "nonnegative Wigner–Ville distribution (NN-WVD)" for displaying the decomposition results of parametric TFRs. The initial impetus for devising the NN-WVD came from the facts that the Morlet wavelet is a special case of both e-chirplet and d-chirplet, and that the WVD of Morlet wavelet is nonnegative and cross-term free. The method of using SAT to construct an NN-WVD is to migrate the values of WVDs of Morlet wavelets to the positions of IFs of the matched elementary functions (e.g., e-chirplet or d-chirplet. The choice of different types of elementary functions depends on the specific application at hand and on the representation properties that are desirable for this application) for different signal components. The relative merits and the usefulness of NN-WVD are twofold: (1) the NN-WVD is nonnegative and cross-term free (the cross-terms in the WVD of elementary function with nonlinearly varying frequencies are annihilated, while the auto-terms are barely affected); (2) the concentration of NN-WVD is identical to that of WVD. Therefore, the NN-WVD is more flexible and advantageous for delineating the time-varying spectral contents of a nonstationary signal.

A fly in the ointment, whether or not we will concede, is that the NN-WVD requires to know the IFs of the signal components in advance. Since we position the calculation of NN-WVD to a post-processing episode for parametric TFR hunting, this is not much of a problem, as the IFs of the signal components are assumed to be given after the calculation of a parametric TFR.

Moreover, our restriction of applications to e-chirplet and d-chirplet transforms in this paper is by no means a limitation. Indeed, the presentation of the SAT principle allows a straightforward extension of its use to many other parametric TFRs, e.g., the ones that use w-chirplets (warbling chirplets) [7], p-chirplets (projective chirplets) [7], splines [39], and the polynomial phase elementary functions [40].

References

[1] Y. Grenier, Time-dependent ARMA modeling of nonstationary signals, IEEE Trans. Acoust. Speech Signal Process. 31 (4) (August 1983) 899–911.

[2] M.G. Hall, A.V. Oppenheim, A.S. Willsky, Time-varying parametric modeling of speech, Signal Process. 5 (3) (May 1983) 267–285.

[3] J. Ängeby, Properties of the structured auto-regressive time–frequency distribution, Proceedings ICASSP1997—IEEE International Conference on Acoustics, Speech, and Signal Processing, vol. 3, Munich, Germany, April 21–24, 1997, pp. 2017–2020.

[4] B. Boashash, P. O'Shea, Polynomial Wigner–Ville distributions and their relationship to time-varying higher order spectra, IEEE Trans. Signal Process. 42 (1) (1994) 216–220.

[5] B. Boashash, B. Ristic, Polynomial time-frequency distributions and time-varying spectra: application to the analysis of multicomponent FM signals and to the treatment of multiplicative noise, Signal Process. 67 (1) (1998) 1–23.

[6] B. Barkat, B. Boashash, Design of higher order polynomial Wigner–Ville distributions, IEEE Trans. Signal Process. 47 (9) (1999) 2608–2611.

[7] S. Mann, S. Haykin, The chirplet transform: physical considerations, IEEE Trans. Signal Process. 43 (11) (1995) 2745–2761.

[8] D. Mihovilović, R.N. Bracewell, Adaptive chirplet representation of signals of time-frequency plane, Electron. Lett. 27 (13) (1991) 1159–1161.

[9] R.G. Baraniuk, D.L. Jones, Wigner-based formulation of the chirplet transform, IEEE Trans. Signal Process. 44 (12) (1996) 3129–3135.

[10] Q. Yin, S. Qian, A. Feng, A fast refinement for adaptive Gaussian chirplet decomposition, IEEE Trans. Signal Process. 50 (6) (2002) 1298–1306.

[11] A. Bultan, A four-parameter atomic decomposition of chirplets, IEEE Trans. Signal Process. 47 (3) (1999) 731–745.

[12] S. Qian, D. Chen, Signal representation via adaptive normalized Gaussian functions, IEEE Trans. Signal Process. 36 (1) (1994) 1–11.

[13] S. Mallat, Z. Zhang, Matching pursuits with time–frequency dictionaries, IEEE Trans. Signal Process. 41 (12) (1993) 3397–3415.

[14] H. Zou, Q. Dai, R. Wang, Y. Li, Parametric TFR via windowed exponential frequency modulated atoms, IEEE Signal Process. Lett. 8 (5) (2001) 140–142.

[15] H. Zou, Q. Dai, K. Zhao, G. Chen, Y. Li, Subspaces of FM^{m}let transform, Sci. China (Series F) 45 (2) (2002) 152–160.

[16] H. Zou, D. Wang, Q. Dai, Y. Li, Real, discrete, and real discrete FM^{m}let transforms, Chinese J. Electron. 13 (1) (2004) 8–11.

[17] H. Zou, D. Wang, Q. Dai, Y. Li, Relations of FM^{m}let transform to some integral transforms, Chinese J. Electron. 13 (2) (2004) 278–282.

[18] Q. Dai, H. Zou, Z. Liu, D. Wang, Y. Li, Properties and convergence analysis of FM^{m}let transform, Sci. China (Series E) 45 (2) (2002) 152–159.

[19] H. Zou, X. Zhou, Y. Li, Time–frequency signal representation with Dopplerlet basis functions (in Chinese), J. Tsinghua Univ. 40 (3) (2000) 52–54.

[20] H. Zou, X. Zhou, Y. Li, Application of Dopplerlet transform to signal retrieval under different contaminating noises (in Chinese), Acta Electron. Sinica 28 (9) (2000) 1–4.

[21] H. Zou, Q. Dai, X. Zhou, Y. Li, Dopplerlet based time–frequency representation via matching pursuit, J. Electron. (China) 18 (3) (2001) 217–227.

[22] H. Zou, Y. Chen, J. Zhu, Q. Dai, G. Wu, Y. Li, Steady-motion-based Dopplerlet transform: application to the estimation of range and speed of a moving sound source, IEEE J. Oceanic Eng. 29 (3) (2004) 887–905.

[23] L. Cohen, T.E. Posch, Positive time–frequency distribution functions, IEEE Trans. Acoust. Speech Signal Process. 33 (1) (February 1985) 31–38.

[24] P.J. Loughlin, J.W. Pitton, L.E. Atlas, Construction of positive time–frequency distributions, IEEE Trans. Signal Process. 42 (10) (October 1994) 2697–2705.

[25] T.H. Sang, W.J. Williams, J.C. O'Neill, Algorithm for positive time–frequency distributions, Proceedings IEEE SP—International Symposium on Time–Frequency and Time-Scale Analysis, Paris, France, June 18–21, 1996, pp. 165–168.

[26] L. Cohen, Generalized phase-space distribution functions, J. Math. Phys. 7 (5) (1966) 781–786.

[27] L. Cohen, Time–Frequency Analysis, Prentice-Hall, Englewood Cliffs, NJ, 1995.

[28] R.L. Hudson, When is the Wigner quasi-probability density non negative?, Rep. Math. Phys. 6 (1974) 249–252.

[29] K. Kodera, C. de Villedary, R. Gendrin, A new method for the numerical analysis of time-varying signals with small BT values, Phys. Earth Planet Interiors 12 (1976) 142–150.

[30] K. Kodera, R. Gendrin, C. de Villedary, Analysis of time-varying signals with small BT values, IEEE Trans. Acoust. Speech Signal Process. 34 (1986) 64–76.

[31] F. Auger, P. Flandrin, Improving the readability of time-frequency and time-scale representations by the reassignment method, IEEE Trans. Signal Process. 43 (5) (1995) 1068–1089.

[32] L. Cohen, Distributions concentrated along the instantaneous frequency, Proceedings SPIE Int. Soc. Opt. Eng.—Advanced Signal-Processing Algorithms, Architectures, and Implementations, vol. 1348, San Diego, CA, USA, July 10–12, 1996, pp. 149–157.

[33] H. Zou, D. Wang, Q. Dai, Y. Li, Chirplet-based nonnegative time-frequency distribution for FM^{m}let transform, Chinese J. Electron. (2005), accepted for publication.

[34] A. Papandreou-Suppappola, S.B. Suppappola, Adaptive time-frequency representations for multiple structures, 10th IEEE Workshop on Statistical Signal and Array Processing, Pocono Manor, Pennsylvania, August 2000, pp. 579–583.

[35] I. Daubechies, Time–frequency localization operators: a geometric phase space approach, IEEE Trans. Inform. Theory 34 (4) (July 1988) 605–612.

[36] R.R. Coifman, M.V. Wickerhauser, Entropy-based algorithms for best basis selection, IEEE Trans. Inform. Theory 38 (2) (part II), (1992) (special issues), 713–718.

[37] S.B. Chen, D.L. Donoho, M.A. Saunders, Atomic decomposition by basis pursuit, SIAM J. Sci. Comput. 20 (1) (January 1998) 33–61.

[38] P.S. Addison, The Illustrated Wavelet Transform Handbook, Institute of Physics Publishing, Bristol, 2002.

[39] S. Jaggi, W.C. Karl, S. Mallat, A.S. Willsky, High-resolution pursuit for feature extraction, Appl. Comput. Harmonic Anal. 5 (4) (1998) 428–449.

[40] S. Peleg, B. Porat, Estimation and classification of polynomial phase signals, J. Audio Eng. Soc. 36 (4) (1988) 223–231.